Desalination and Water Treatment
www.deswater.com

doi: 10.5004/dwt.2017.20516

71 (2017) 244–260
April

The extent of change in the physicochemical characteristics and pollutants sequestration of date palm stones after microemulsion modification

Nasir M.A. Al Lagtah[a,b,*], Mohammad N.M. Ahmad[c], Ahmad B. Albadarin[d,e]

[a]*School of Engineering and Physical Sciences, Heriot-Watt University Dubai Campus, Dubai International Academic City, P.O. Box: 294345, Dubai, UAE, Tel. +971 4 435 8794; email: n.al_lagtah@hw.ac.uk*
[b]*School of Chemical Engineering and Advanced Materials, Newcastle University, 537 Clementi Road, #06-01, 599493, Singapore*
[c]*Department of Chemical and Petroleum Engineering, Faculty of Engineering and Architecture, American University of Beirut, Beirut, Lebanon, email: ma258@aub.edu.lb*
[d]*Department of Chemical and Environmental Sciences, Bernal Institute, University of Limerick, Ireland, email: ahmad.b.albadarin@ul.ie*
[e]*School of Chemistry and Chemical Engineering, Queen's University of Belfast, Belfast, UK*

Received 21 June 2016; Accepted 18 January 2017

ABSTRACT

Date palm stones (DPS) can be used as inexpensive adsorbents, which are inferior to commercial activated carbons, but their potential low cost makes them competitive. The promising microemulsion modification process has the potential to improve the adsorption performance of DPS. In this study, the extent of change in the physicochemical properties of DPS due to the microemulsion modification and the removal of methylene blue (MB) and hexavalent chromium Cr(VI) have been investigated. Fourier transform infrared (FTIR) analysis showed that DPS surface contains non-polar/hydrophobic and polar/hydrophilic functional groups, whilst the microemulsion attachment to DPS surface is either by its hydrophilic or by its hydrophobic part. The microemulsion modification increased the basicity of the surface, causing an increase in the zero point of charge (pH_{ZPC}) and significantly reduced the surface area and total pore volume of DPS. The sequestration of MB and Cr(VI) from aqueous solutions by DPS and microemulsion-modified DPS (MDPS) showed that the solution pH had the most noticed effect on Cr(VI) removal. The sequestration of MB by DPS was endothermic but changed to exothermic after modification, whilst the sequestration of Cr(VI) by both solid adsorbents was endothermic. The sequestration capacity of MB was higher but lower for Cr(VI) by MDPS compared with DPS. Overall, microemulsion modification of DPS had changed their physicochemical properties and altered their capacity of sequestrating different pollutants from aqueous solutions.

Keywords: Date palm stones; Microemulsion modification; Surface characterisation; FTIR analysis; Sequestration

1. Introduction

Freshwater counts for <1% of the earth's water sources and is increasingly under pressure due to the fast growth of population, technological development, urbanisation and economic growth [1]. Pollution decreases the supply of usable water and increases the cost of purifying it. Two of the most hazardous water pollutants are heavy metals and dyes. Heavy metals, such as chromium, are regarded as major inorganic pollutants due to their notable toxicity, even at relatively minimal degrees of exposure. These heavy metals are presented in the effluents of petroleum refining, textile, electroplating, fertilizers and paper manufacturing industries [2]. Dyes are chemical substances that are used to impart colour to fabrics or surfaces. Synthetic dyes are complex organic molecules that are widely used in the manufacturing industries of textile,

* Corresponding author.

leather tanning, paper and food. They can cause considerable environmental pollution and serious health risks [3].

Liquid-phase adsorption is a process that is widely applied to treat polluted waters. Proper design of the adsorption process produces a high-quality treated effluent and hence offers an appealing option for the treatment of contaminated waters, particularly if the adsorbent is inexpensive [4]. Commercial activated carbon (CAC) is the most effective adsorbent because of its structural characteristics and porosity that gives it a large surface area. However, CAC is quite expensive and non-selective, and requires complexion agents to improve its removal performance. The need for more economically viable substitutes to CAC has encouraged the search for adsorbents that are inexpensive, are easily obtainable and require little processing. One of the most viable and promising low-cost adsorbents are agrowastes, which are produced from plentiful waste materials and present a comparable efficiency and selectivity [5].

Date palm is a key agricultural produce in the Middle East and North Africa, and plays a central role in the culture and tradition of the people of these regions. Date palm stone (DPS) forms an integral part of the date fruit, which accounts up to 15% of its total weight. At present, DPS is mainly used for animal feeding because it is rich in protein, fat, dietary fibre and antioxidants [6]. The use of date palm as an adsorbent has been reviewed by Ahmad et al. [7]. They reported that natural and activated DPS have been used to remove heavy metals, dyes and phenolic compounds from aqueous solutions. However, they have not reported any previous work investigating the effect of microemulsion modification on the properties and the sequestration potential of DPS.

Microemulsion is a heterogeneous system made up of a mixture of immiscible liquids i.e. water, hydrocarbons and co-surfactants. Typical co-surfactants are short chain alcohols (i.e. ethanol to butanol), medium chain alcohols, amines or acids [8]. Microemulsion modification was applied mostly to clay, zeolites and diatomite to improve their ability to remove heavy metals and dyes [9–13]. To the best of our knowledge, there has been no previous publication that investigated the use of microemulsion-modified agrowastes to remove pollutants from aqueous solution, apart from Al-Ghouti et al. [8]. However, they have not thoroughly investigated the effect of microemulsion modification on the surface characteristics of DPS. Therefore, this paper will investigate the extent of change in the physical and chemical characteristics (specific surface areas, pore volumes, surface acidity and basicity, Fourier transform infrared [FTIR] and scanning electron microscopy [SEM] analysis) and sequestration of methylene blue (MB) and Cr(VI) under different experimental parameters (solution pH, adsorbate initial concentration and solution temperature) of DPS due to microemulsion modification.

2. Materials and methods

2.1. Chemicals

All the chemicals used in this work were of analytical grade (Sigma-Aldrich, UK). The aqueous solutions of the adsorbates were prepared from MB ($C_{16}H_{18}N_3S^+Cl^-$) and potassium dichromate ($K_2Cr_2O_7$). The microemulsion was prepared by mixing 10 wt% surfactant (saponified coconut oil) and 25 wt% aqueous phase (deionised water). Coconut oil was saponified by an ASTM standard procedure (ASTM D-5558/1995) to form $CH_3(CH_2)_{10}COO^-Na^+$. The mixture was then mixed with 40 wt% co-surfactant (isoamyl alcohol, 99%) and 25 wt% oil phase (heavy distillate). Due to the spontaneous formation of microemulsion, it can be prepared in one step by simply mixing the constituents. The addition order of the constituents is not considered a critical factor for the preparation of the microemulsion, but it can influence the time required to obtain equilibrium. This time will increase if the co-surfactant is added to the organic phase, due to its greater solubility in this phase, and hence, will prevent its diffusion in the aqueous phase. Solutions of sodium hydroxide and hydrochloric acid were prepared for adjusting the solution pH and as eluents.

2.2. Adsorbents

DPS were obtained from a date-processing factory in Jordan. They were collected and washed with deionised water, dried in an oven at 105°C for 3 h and crushed into a dark brown powder. The powder was sieved, and the smallest particle size of 125–300 μm was used to prepare the microemulsion-modified DPS (MDPS) and for the batch adsorption experiments. To prepare MDPS, 10 ± 0.1 g of DPS and 20 ± 0.5 mL of microemulsion were mixed and then dried at 65°C for 48 h.

2.3. Physical and chemical characterisation of adsorbents

Surface characterisation of DPS and MDPS included determining the total, external and micropore specific surface areas, total pore, micropore and mesopore volumes, and the average pore size. Adsorption/desorption isotherms of N_2 were generated using a gas porosimeter (Nova 4200, Quantachrome Instruments, UK). The total surface area (A_{BET}), total pore volume (V_{total}) and average pore size for each adsorbent were estimated from the generated N_2 adsorption isotherms by Brunauer–Emmett–Teller (BET) isotherm as shown in Eq. (1):

$$\frac{P/P_0}{V_n(1-P/P_0)} = \frac{1}{V_m c} + \frac{c-1}{V_m c}\left(P/P_0\right) \quad (1)$$

where V_n (mL STP g^{-1}) is the volume of nitrogen adsorbed at pressure P; P_0 is the standard vapour pressure of the liquid at the temperature of experiment (77 K); V_m (mL STP g^{-1}) is the equivalent volume to an adsorbed monolayer and c is the BET constant linked to the adsorption molar energy of the first monolayer (i.e. a representation of the scale of the adsorbent–adsorbate interaction energy). The total pore volume (V_{total}) was estimated from the volume of nitrogen held at the relative pressure $P/P_0 = 0.98$ (maximum relative pressure).

The *t*-plot method was applied to estimate the micropore volume (V_{micro}), micropore surface area (A_{micro}) and the external surface area (A_{ext}) of the adsorbents. The thickness of the adsorbed layer (t) is a function of the gas relative pressure (P/P_0) and is calculated using Harkins and Jura equation:

$$t\ (\text{nm}) = 0.1\left[\frac{13.99}{0.034 - \log(P/P_0)}\right]^{0.5} \quad (2)$$

The amount of nitrogen adsorbed (V_n) is plotted against t, and the plot usually gives two distinct linear regions, and therefore, two straight lines can be drawn for these two regions. The slope of the first linear line passing through the origin can be used to calculate the micropore surface area (A_{micro}), whilst the slope of the second straight line is used to calculate the external surface area (A_{ext}). Those two areas are calculated using Eq. (3):

$$A = \left(V_m a_m NA\right)/\left(mV_L\right) \tag{3}$$

where V_m equals 0.354 multiplied by the slope; a_m is the cross-sectional area occupied by each nitrogen molecule (0.162 nm^2); NA is Avogadro's number (6.023 × 10^{23} molecule mol^{-1}); m is weight of the sample (g) and V_L is the molar volume of nitrogen gas (22,414 mL STP).

The intercept of the second line gives the volume of micropores (V_{micro}). However, this intercept will be at STP conditions and, therefore, should be modified to present the values in the unit of mL g^{-1} by applying the following formula:

$$V_{micro} = \left(\text{Intercept}/V_L\right)\left(MW/\rho_L\right) \tag{4}$$

where MW (g mol^{-1}) is the molecular weight of the adsorbed nitrogen, and ρ_L is liquid nitrogen density at 77 K (0.807 g mL^{-1}). The volume of mesopores (V_{meso}) was obtained by subtracting the volume of micropores from the total pore volume. The pore size distributions of DPS and MDPS were determined from N_2 adsorption/desorption data by applying a simplified method proposed by Dollimore and Heal [14].

The pH of the suspension ($pH_{suspension}$) was evaluated by mixing the appropriate weights of an adsorbent and deionised water in a glass jar to form 10% (w/w) suspension. This suspension was constantly shaken for 24 h at room temperature (20°C ± 2°C). The pH was measured several times until a constant value was reached. The jar was then removed and left until the adsorbent's particles settled, and after that, the final value of the suspension pH was recorded. The pH measurements were duplicated, and the average value was regarded as the $pH_{suspension}$.

The simple and reliable alkalimetric titration method had been used to evaluate the surface charges of the adsorbents. This method started with preparing a series of adsorbent samples (0.5 ± 0.1 g) and then mixed with varying amounts of 0.25 M HCl and 0.25 M NaOH solutions to give different pH values. The acid or alkaline solutions were cautiously transferred using 1.00 mL micropipette. Afterwards, they were diluted to a final volume of 25 ± 0.5 mL with deionised water in a 60-mL glass jar. The bottles were then tightly sealed and shaken for 24 h at room temperature (20°C ± 2°C). After that, the equilibrium pH of the solutions was measured, and the concentrations of H^+ and OH^- were calculated. Surface charge density (σ) of each solution was calculated, and a plot of σ vs. pH was created. The value of zero point of charge, pH_{ZPC}, refers to the pH value where zero-net adsorption of H^+ and OH^- ions has been achieved. The intersection of the curve with x-axis at σ equals zero gives pH_{ZPC} [15].

Simple titration technique was used to determine the basicity and acidity of the adsorbent surface. 0.5 ± 0.1 g of the adsorbent was mixed with 50 ± 0.5 mL of 0.01 M NaOH (for acidity) or 0.1 M HCl (for basicity), and constantly agitated until reaching equilibrium. The mixture was filtered and back titrated with 0.1 M HCl or 0.01 M NaOH to offset the excess of sodium hydroxide or hydrochloric acid, respectively. Phenolphthalein 1% was used as an indicator. The acidity of the surface, measured in mol g^{-1}, was determined based on the concentration of NaOH in the solution calculated from the amount of HCl used in titration and vice versa for determining the basicity of the surface [16].

Characterisation of the surface of the adsorbents by FTIR method involves the observation of perturbations of surface functional groups. Infrared spectra were collected by using an FTIR-Perkin Elmer Spectrophotometer RXI instrument (PerkinElmer, USA). The texture of the adsorbents had been examined using SEM using JEOL-JSM 6400 scanning microscope.

2.4. Adsorption equilibrium experiments

Batch experiments were undertaken to study the effect of microemulsion modification on the sequestration of MB dye and Cr(VI) under different experimental parameters. The initial pH of the pollutant solutions was adjusted to the required value (a range of 2–10) by adding either 1 M HCl or 1 M NaOH. The initial concentrations of MB were 50, 100, 150, 200, 300, 500, 700 and 900 mg L^{-1}. For Cr(VI), the initial concentrations were 1, 3, 5, 10, 20, 30, 40 and 50 mg L^{-1}. The adsorption equilibrium studies were conducted at various solution temperatures (20°C, 30°C, 45°C and 60°C) in a water bath/shaker. For all experiments, duplicate samples were measured, and the standard error in the readings was <5%. The experiments were completed in 50-mL glass jars, where mixtures of 0.025 g of an adsorbent and 25 mL of each pollutant under the investigated parameters were constantly agitated at 150 rpm for 96 h to reach equilibrium at room temperature (20°C ± 2°C). After that, the jars were removed, and the mixtures were filtered to remove the spent adsorbent. The initial fraction of the remainder was dismissed to reduce the effects of adsorbed pollutants onto the filter paper. The removal percentage of each pollutant was calculated using the following equation:

$$\text{Removal (\%)} = 100\left(C_0 - C_e\right)/C_0 \tag{5}$$

with C_0 and C_e (mg L^{-1}) are the liquid-phase concentration of each pollutant at initial and equilibrium conditions, respectively.

The initial and final MB concentrations were determined using a PerkinElmer UV–Vis spectrophotometer. The initial and equilibrium concentrations of chromium were determined using inductively coupled plasma (ICP) after diluting the filtrate to an adequate concentration.

The adsorption capacity (q_e, mg g^{-1}), which is the amount adsorbed of each pollutant in 1 g of adsorbent, was calculated according to Eq. (6):

$$q_e = \left(V/m\right)\left(C_0 - C_e\right) \tag{6}$$

where V is the volume of solution (L), and m is the mass of the adsorbate (g).

The relation between equilibrium solid and liquid concentrations is described by an adsorption isotherm. Langmuir adsorption isotherm is expressed as:

$$q_e = \left(q_{\max} b C_e\right) / \left(1 + b C_e\right) \quad (7)$$

where $q_{\max}$ (mg g^{-1}) is the maximum monolayer adsorption capacity, and b (L mg^{-1}) is a constant related to the free energy of adsorption.

Non-linear regression of adsorption equilibrium data was applied to fit the experimental data to Langmuir adsorption isotherm. Non-linear regression involves minimising the difference between the experimental q_e and the predicted value (q_{pred}) using different well-established error functions. These error functions are the sum of the square errors (SSE), hybrid fractional error function (HYBRID), Marquardt's percent standard deviation (MPSD) and root mean square error (RMSE). Applying different error functions will produce different sets of isotherm parameters. Thus, it is essential to apply a method that allows a direct comparison among the scaled errors and hence identifies the set of isotherm parameters that provides the closest fit to the measured data. This method is called the sum of normalized errors (SNE) [17].

The non-linear regression software used in this work is GAMS®, which is a graphic user interface (GUI) that embodies the use of optimisation subroutines such as the KNITRO®, which is based on the successive quadratic programming (SQP) algorithm. Non-linear regression can be achieved by Microsoft Excel Solver®, which is based on the generalised reduced gradient (GRG) algorithm. However, the SQP method requires much smaller evaluation time because of its second-order convergence [18].

The desorption experiments were carried out using different eluents (deionised water, 1 M NaOH and 1 M HCl) in order to determine the most appropriate eluent to regenerate the adsorbent to be used in multiple adsorption–desorption cycles. After the equilibrium adsorption experiment, the adsorbent was separated by filtration and washed with deionised water to remove any remaining adsorbate. Afterwards, adsorbent was mixed with 25 mL of each eluent solution. The suspensions were shaken for 24 h, filtered and analysed to find out the concentration of the pollutants after desorption. Desorption percentage can be calculated using the following equation:

$$\text{Desorption (\%)} = 100\left(\frac{\text{amount pollutant desorbed}}{\text{amount pollutant adsorbed}}\right) \quad (8)$$

3. Results and discussion

3.1. Physicochemical characteristics of DPS and MDPS

It is well known that the surface characteristics of an adsorbent can significantly influence its potential to remove pollutants from aqueous solutions [16]. DPS mainly consists of three components: cellulose, hemicellulose and lignin, and their average percent are 17.5%, 11.0% and 42.5% dry weight, respectively [8]. The elemental analysis of DPS gives 45.3%–45.8% C, 46.6%–47.2% O, 5.6%–6.3% H, 0.8%–1.0% N and 0.2%–0.8% S. This elemental analysis shows the existence of heteroatoms (O, N and S) and hence the presence of functional groups, mainly oxygen-containing surface groups. These oxygen functional groups, along with the delocalised electrons of the DPS structure, determine DPS surface acidity or basicity [19]. Therefore, it is very important to understand the surface chemistry of DPS to assess in depth its overall characteristics and functional groups contributing to its acidity and basicity.

3.1.1. Surface charge density and pH_{ZPC}

DPS surface is expected to exhibit electrical charge properties that will strongly influence the sequestration of ionic and polar pollutants from aqueous solutions. Therefore, the surface charge of DPS must be counterbalanced in the aqueous phase to maintain an electroneutrality. Therefore, an electrical double-layer will exist at the DPS–water interface. The hydroxyl groups present on the surface of DPS can gain or lose a proton, resulting in a surface charge that varies with changing solution pH. It is possible that the average surface charge to become neutral and the solution pH that establishes such neutral charge is called pH_{ZPC}. Furthermore, pH_{ZPC} is useful in predicting the nature of the surface reaction since it is a function of the acidity and the electrostatic field strength of the adsorbent [20].

Surface charge densities, σ, of the DPS and MDPS as a function of the solution pH are shown in Fig. 1. The intersection of the curve with x-axis is pH_{ZPC}. For DPS, pH_{ZPC} is 4.42, whilst it is 5.14 for MDPS. For initial solution pH values below pH_{ZPC}, the overall surface charge of each adsorbent will be positive and attracts anions. For initial solution pH above pH_{ZPC}, the surface of each adsorbent will be bearing an overall negative charge attracting cations [20].

The $pH_{suspension}$ was found to be 4.49 for DPS, which was very similar to pH_{ZPC} and that would indicate that $pH_{suspension}$ could be taken as equivalent to the pH_{ZPC}, as has been demonstrated by previous investigators [18]. However, the $pH_{suspension}$ for MDPS was 6.87 and higher than pH_{ZPC}, which would be due to the possibility of sodium ion dissociation from microemulsion molecules ($CH_3(CH_2)_{10}COO^-Na^+$), and the presence of Na^+ ions would increase the overall value of solution pH.

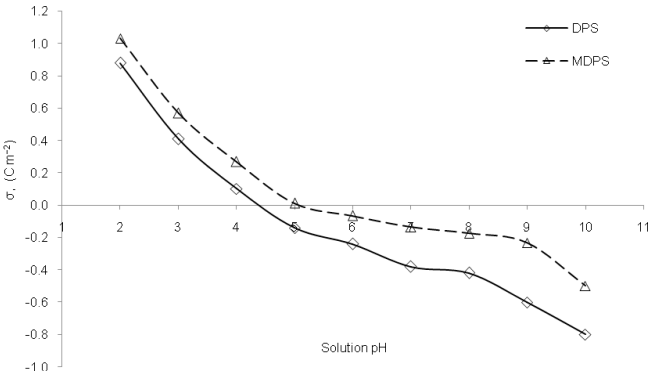

Fig. 1. Surface charge density and pH_{ZPC} of DPS and MDPS (experimental conditions: mass of adsorbent = 0.5 g, volume of solution = 50 mL, equilibrium time = 24 h, temperature = 20°C and shaking speed = 100 rpm).

If the microemulsion droplets are presumed to be spherical, then high surface charge is expected to produce sufficient electrostatic repulsion between the droplets to maintain the stability of the system [21]. It could be noticed from Fig. 1 that all the values of σ for MDPS were higher than those for DPS, indicating that the addition of microemulsion produced a stable adsorbent.

3.1.2. Surface acidity and basicity

The surface of adsorbents may have acidic or basic chemical functional groups. These groups will influence the sequestration of pollutants from aqueous solutions. The acidity and basicity of an adsorbent usually refer to acidic and basic groups existing on its surface. Agrowastes, such as DPS, contain different functional groups. The most common groups are: carboxyl, carbonyl and phenolic groups. Agrowastes with low oxygen content show basic properties and anion exchange behaviour, whilst agrowastes with high oxygen content show acidic properties and cation exchange behaviour [22]. The surface acidity and basicity of DPS and MDPS are listed in Table 1.

Table 1 shows that DPS has higher acidic characteristics than its basic characteristics. The acidity of an adsorbent is predominantly governed by the presence of carboxylic groups. Carboxylic groups are already presented in lignin, which accounts for 42.5% of DPS, and these groups are able to act as a source of ion exchange and can be utilised to evaluate the adsorption mechanisms of dyes and heavy metals [23]. On the other hand, the basicity of MDPS was higher by 50%, which is due to the basicity of the functional group ($RCOO^-$) on the surface of MDPS. The higher basicity of MDPS would explain the higher values of pH_{ZPC} and $pH_{suspension}$ than those of DPS.

3.1.3. FTIR and SEM analysis

The characterisation of the different surface functional groups of DPS can be carried out by FTIR analysis. Surface functional groups connect polymer chains by hydrogen bonds to give structural support and perform a key part in the sequestration processes [22]. Therefore, it is important to identify the surface functional groups of DPS before and after microemulsion modification to examine the extent of change in surface chemistry. The results of FTIR analysis for DPS and MDPS are presented in Fig. 2.

The core constituents of DPS are cellulose, hemicelluloses and lignin. These constituents have hydroxyl groups (CH–O–H) with bands around 3,350 and 1,050 cm^{-1}. For DPS, broader and more intense bands appeared around 3,460 cm^{-1}, suggesting that cellulose and lignin (which contains a higher density of hydroxyl groups) are more freely vibrated by infrared energy resulting in stretching O–H bond because of some loss of hemicelluloses and extractives from DPS during water washing [23].

Lignin and hemicellulose contain carboxyl groups (–C(=O)OH) with characteristic infrared bands around 1,740 and 1,660 cm^{-1}, which are associated with aliphatic and aromatic compounds, respectively. For DPS, a very sharp and intense band is noticed at 1,744 cm^{-1} as a result of free carbonyl group (–C=O) stretching within the carboxylic groups found in xylans (hemicellulose) [24]. The broad band around 1,610 cm^{-1} is associated with the existence of negatively charged carboxylate ion (–(C=O)–O^-) attributed to lignin in DPS. Also, nitrogen-based functional groups (e.g. amine and amide) show characteristics bands around 1,610 cm^{-1}, which are attributed to (C=C) aromatic rings stretching within the lignin that contains higher density of nitrogen-based groups [25]. Stretching bands are often divided into two divisions: symmetric stretch (where the two C–H bonds stretch in the same direction) and asymmetric stretch (where the two C–H bonds stretch in the opposite directions). The asymmetric stretch is slightly of higher energy and hence has higher wave number. That can be seen in Fig. 2 where two intense characteristic bands at 2,925 and 2,854 cm^{-1} corresponding to the asymmetrical and symmetrical stretching vibrations of C–H bond, respectively [26].

The surface functional groups of DPS can be classed into two major categories: non-polar (hydrophobic) functional groups (e.g. aromatic rings and methylene groups) and polar (hydrophilic) functional groups (e.g. hydroxyl, carboxyl and carbonyl groups) [7]. The microemulsion molecules have two parts: hydrophilic head and hydrophobic tail. Therefore, it is possible for the microemulsion to attach to DPS surface by hydrophobic interaction between the microemulsion tail and DPS hydrophobic functional groups. Consequently, the negative charge of the microemulsion head will be towards the solution. Another interaction possibility is due to the hydrophilic bonding between the negatively charged head of the microemulsion molecules and the hydrophilic groups of DPS. However, the carboxyl groups are negatively charged and will not bond with the head of the microemulsion and instead such bonding will be with polar hydroxyl

Table 1
Acidity and basicity values, solution pH_{ZPC} and solution $pH_{suspension}$ of DPS and MDPS

Adsorbent	DPS	MDPS
Acidity, C_A (mmol g^{-1})	0.681	0.693
Basicity, C_B (mmol g^{-1})	0.415	0.616
Solution pH_{ZPC}	4.42	5.14
Solution $pH_{suspension}$ (10 wt%, 20°C)	4.49	6.87

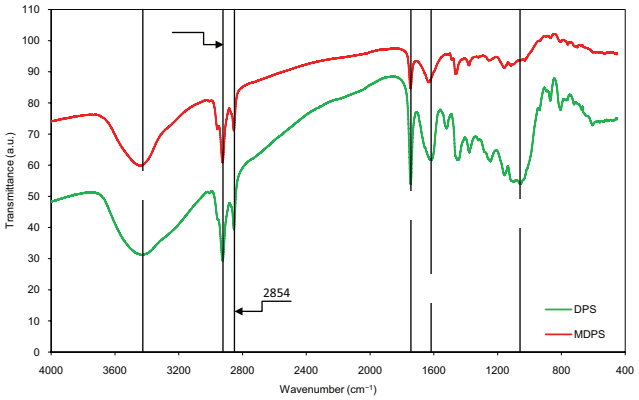

Fig. 2. FTIR spectra of DPS and MDPS adsorbents.

and carbonyl groups. These arrangements may lead to a multilayer adsorption of the microemulsion on the surface of DPS. To examine the extent of change to DPS surface due to the microemulsion modification, MDPS was subjected to FTIR analysis (Fig. 2). Microemulsion modification resulted in the appearance of shifted bands at 1,633 cm^{-1}, referring to (COO^-), and at 1,462 cm^{-1}, referring to stretching in $–CH_3$ in lignin. That means a chemisorption occurred, where carboxylic acids (from saponified coconut oil) have been adsorbed on the surface of DPS increasing the concentration of carboxylate groups. After microemulsion modification, the absorption band at 3,460 cm^{-1} became broader because of the excess water molecules attached to OH groups [27]. On the other hand, most of the absorption bands that disappeared after microemulsion modification were those of aromatics and O–H bonds of carboxylic acids within lignin, almost eliminating its hydrophobic nature. The bands of methylene groups contracted and became less stretched after microemulsion modification. That means that the microemulsion attached to DPS surface by H–C–H bond, which is hydrophobic. Another band that became less intense was that at 1,744 cm^{-1} attributed to xylans. Xylans have hydrophilic and hydrophobic properties [28], and consequently, the microemulsion molecule interacts with xylan in the DPS surface either via its head or via its tail. However, because of the large size of microemulsion molecules, not all methylene groups and xylans will be linked up, and hence few still exist on MDPS surface, explaining why FTIR analysis of MDPS still shows absorption bands of methylene groups and xylans.

In conclusion, the FTIR analysis of MDPS surface indicates that its nature cannot be simply described either as hydrophilic or hydrophobic since the interactions between the microemulsion molecules and DPS surface are either hydrophilic or hydrophobic. Moreover, there is still a possibility of incomplete coverage of the whole surface of DPS since the microemulsion molecules are considered large in size.

Fig. 3 shows the surface morphology of DPS and MDPS. The SEM image of DPS surface showed that it is porous and heterogeneous. After modification, the SEM image of MDPS showed the formation of spherical agglomerates on the surface. At the start of DPS modification, the microemulsion concentration is low and hence arranges itself parallel to DPS surface, occupying the corresponding plan projection area. As the microemulsion concentration increases and becomes greater than the critical micelle concentration, aggregates of two-and three-dimension micelles will be formed on DPS surface. These agglomerates will take the spherical shape because it is thermodynamically more stable than other shapes [29]. Therefore, the mechanism of the microemulsion modification of DPS starts through hydrophilic interaction, and as the microemulsion concentration increases, the modification happens mainly through hydrophobic interaction. The attachment of the microemulsion system to DPS surface is illustrated in Fig. 4. The microemulsion molecules interact electrostatically and align with their charged heads towards the surface of the DPS (circled section in Fig. 4) or through the growth of aggregates on DPS surface (Fig. 3).

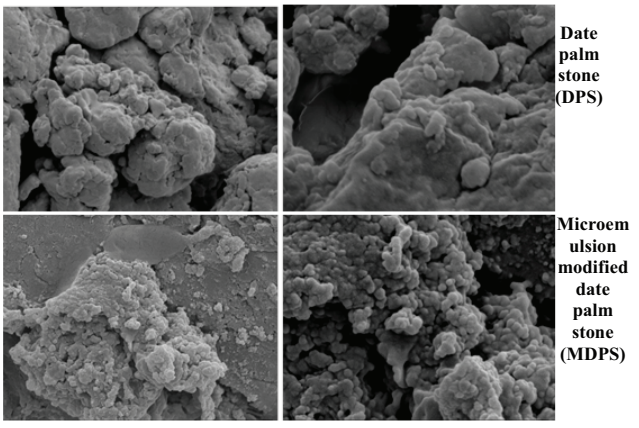

Fig. 3. Scanning electron microscopy (SEM) images of DPS (top images) and MDPS (bottom images). (Note: The magnification of the left images is X20,000 and for the right images is X50,000 of original A6 photo.)

3.1.4. Adsorbents specific surface area, pore volume and pore size distributions

The adsorptive properties of an agrowaste depend mainly on its physical characteristics (specific surface area, pore volume and pore size distribution), together with its surface chemistry. It is expected that microemulsion modification will change the surface area, porosity and accessibility to internal sites of DPS [27]. To investigate the extent of such a change, the N_2 adsorption–desorption isotherms of DPS and MDPS (not shown) were analysed, and it was found that they can be classified as type III isotherm, which is a rare isotherm and is commonly linked to water vapour adsorption. In this type of isotherms, the interactions between the adsorbent and adsorbate are weak [16]. The two adsorbents also showed low-pressure hysteresis loops, and their desorption branches went parallel to the

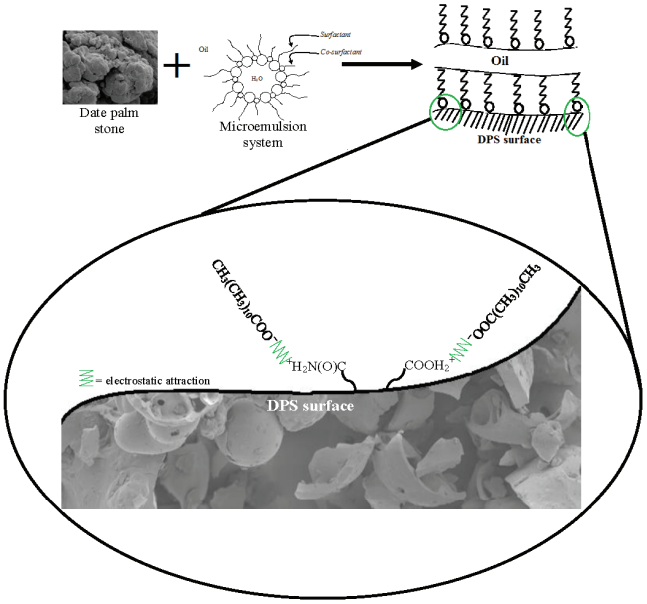

Fig. 4. Graphic presentation of the electrostatic interaction between microemulsion system and DPS surface.

adsorption curves. This behaviour is usually associated to the swelling of the adsorbent particles. This swelling is not completely elastic, and some N_2 molecules get entrapped within the adsorbent and hence cannot escape during desorption phase. The lower end of the two hysteresis loops occurred at relative pressure of 0.35, suggesting the presence of ink-bottle effect. However, the very narrow hysteresis loops indicate the existence of lesser amount of porous spaces and ink-bottle pores [14].

The BET equation (Eq. (1)) was applied to the linear ranges of the two N_2 adsorption isotherms, and Table 2 summarises the estimated values of A_{BET}, V_{total} and average pore size for DPS and MDPS. It is clear that the A_{BET} of DPS significantly decreased after the microemulsion modification, indicating a considerable structure change. The value of BET constant (c) for DPS was the highest, attributed to the existence of micropores. Moreover, V_{total} of MDPS was 6.7 times smaller than that of DPS. This decrease can be related to the possible blocking of micropores by the large-size microemulsion molecules.

The pore size distributions of DPS and MDPS are shown in Fig. 5. The pore size distribution of DPS shows more noticeable existence of micropores compared with MDPS. The main peak representing the average pore size of DPS is at 1.16 nm and can be considered narrow. After microemulsion modification, the peak shifted to the right and became wider. The average pore size of MDPS, responding to this shifted peak, is 2.20 nm and is identical to the reported value in Table 3. Fig. 5 also shows that most of DPS pores are micropores, whilst the majority of MDPS pores are mesopores. The main distinction between the adsorption in micropores and in larger pores (mesopores or macropores) is that the sizes of micropores are comparable with those of the adsorbate molecules. Therefore, the adsorption in micropores is a pore-filling process, in which their volume is the main controlling factor. On the other hand, the presence of mesopores and macropores suggests the possibility of multilayer adsorption behaviour [34].

The t-plot method was applied to determine A_{micro}, A_{ext}, V_{micro} and V_{meso} of DPS and MDPS, and their values are shown in Table 3, along with their estimated values of total pore volume and average pore size using Dollimore and Heal method. The comparison of the t-plot of DPS and MDPS (not shown) revealed some interesting differences. The t-plot of DPS was relatively simple in form, having two easy-to-distinguish linear portions; whilst the t-plot of MDPS appeared to only have one linear range, which strongly deviates from ideal t-plot. This deviation is associated to the large size of microemulsion molecules that would not diffuse into the micropores, and thusly, the attachment of the microemulsion to DPS surface happened mainly inside the mesopores, indicating that the external surface area will be almost equal to the total area.

The contribution of micropores to the total surface area of DPS (~74%) is considerably significant, even that A_{BET} of DPS can be considered small if compared with the surface area of CACs that ranges from 500 to 2,000 $m^2\ g^{-1}$. However, agrowastes usually have small surface areas [5], and A_{BET} of DPS could be considered relatively high among them. Mesopores have the utmost influence on the sequestration of organic pollutants such as dyes since they permit the access of dyes within the adsorbent structure [30].

Table 2
Surface area, monolayer capacity, total pore volume and average pore size of DPS and MDPS using BET analysis

Adsorbent	DPS	MDPS
BET specific surface area (A_{BET}) ($m^2\ g^{-1}$)	80.49	8.258
c	2.79	1.03
Total pore volume (V_{total}) ($m^3\ g^{-1}$)	7.261E-02	1.083E-02
Average pore size (nm)	1.80	2.21

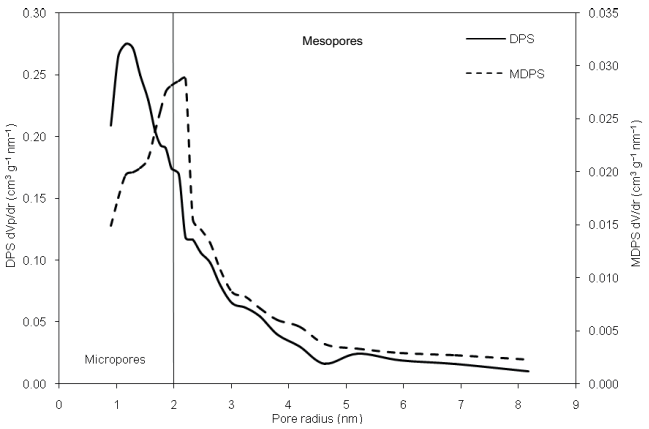

Fig. 5. Pore size distribution of DPS and MDPS determined by Dollimore and Heal method.

3.2. Batch adsorption equilibrium studies

3.2.1. Effect of solution pH

The effect of microemulsion modification on the adsorption equilibria of MB and Cr(VI) at different solution pH and temperatures is summarised in Appendix A, which contains supplementary figures for the removal efficiencies

Table 3
Total area, micropore volume, micropore area, mesopore volume, mesopore area, total pore volume, average pore radius, total pore volume and percentage of micropores and mesopores of DPS and MDPS

	DPS	MDPS
Total area[a] ($m^2\ g^{-1}$)	61.5	6.96
Micropore area[a] (A_{micro}) ($m^2\ g^{-1}$)	45.3	0.368
External surface area[a] (A_{ext}) ($m^2\ g^{-1}$)	16.2	6.60
Micropore volume[a] (V_{micro}) ($cm^3\ g^{-1}$)	4.58E-02	1.04E-04
Mesopore volume[a] (V_{meso}) ($cm^3\ g^{-1}$)	2.69E-02	1.07E-02
Total pore volume[b] ($cm^3\ g^{-1}$)	7.30E-02	1.09E-02
Micropore volume percentage[c] (%)	63.0	1.00
Mesopore volume percentage[c] (%)	37.0	99.0
Average pore size[b] (nm)	1.84	2.15

[a]Calculated by t-plot method.
[b]Calculated by Dollimore and Heal method.
[c]Based on the V_{total} calculated by BET equation.

of these pollutants by DPS and MDPS and, more importantly, the extent of change in these efficiencies due to microemulsion modification.

The effect of microemulsion modification on MB removal efficiency at different solution pH is shown in Fig. A1. The removal of MB by DPS was minimal at solution pH of 2.0 and increased with the increase of solution pH. Microemulsion modification has the beneficial effect of changing the hydrophobic character of DPS surface, resulting in an increase in the removal of the highly hydrophobic molecules of MB. The microemulsion modification almost covered DPS surface with surfactants ($RCOO^-Na^+$), and thusly, the positively charged MB molecules will exchange with Na^+ ions. Moreover, Fig. A1 shows that microemulsion modification almost eliminated the effect of solution pH on MB removal efficiency at solution pH >5.14 (pH_{ZPC} of MDPS). However, the high removal efficiency of MB at solution pH of 4.0 might be related to the affinity of MB molecules onto MDPS surface or their capture by microemulsion micelles.

The effect of solution pH on the removal of Cr(VI) by DPS and MDPS (Fig. A2) showed a total different behaviour. Cr(VI) removal by DPS and MDPS depended immensely on solution pH. High solution acidity results in the formation of more polymerised Cr oxide species, whilst the adsorbent surface becomes highly protonated and favours the uptake of chromium in these anionic forms. With increasing solution pH, the degree of protonation of the surface reduces gradually, and hence, Cr(VI) removal decreases due to the competition between OH^- and dominant chromate species (CrO_4^{2-}) ultimately leading to low removal efficiencies [23]. The removal efficiency of Cr(VI) by MDPS reached its highest value at solution pH of 2.0; at which the predominant species of chromium would be $Cr_3O_{10}^{2-}$ and $Cr_4O_{13}^{2-}$, whilst the surface of MDPS is highly protonated and favours the uptake of these anionic species. However, the highest removal efficiency by MDPS was lower than the highest removal efficiency by DPS, which was at solution pH of 3.0. This shift in solution pH is because that microemulsion droplets have covered DPS surface and almost eliminated the role of surface functional groups by replacing them with the surfactant groups. Therefore, the removal of Cr(VI) by MDPS is mainly related to the protonation of the surface, whilst the presence of lignin in DPS will further enhance the removal process under acidic conditions. Fig. A3 shows the extent of change in MB and Cr(VI) removal efficiencies at different solution pH due to microemulsion modification. For MB, microemulsion modification increased its removal efficiency regardless of the solution pH. In contrast, the negative effect of microemulsion modification on Cr(VI) removal is very noticeable, where the removal by MDPS at solution pH ≥ 3 was lesser by half than that by DPS.

3.2.2. Effect of solution temperature

The removal efficiencies of MB by DPS and MDPS at different solution temperatures are shown in Fig. A4. The removal efficiencies of MB by DPS increased from 86.5% to 95.0% as the solution temperature increased from 20°C to 60°C, indicating that MB uptake by DPS was endothermic. In contrast, MB uptake by MDPS slightly decreased (by only 2.5%) for the same range of temperatures, indicating that microemulsion modification has changed the nature of MB sequestration process to exothermic. Even though, it seems that microemulsion modification almost eliminated the effect of solution temperature on MB sequestration. The effect of solution temperature on Cr(VI) uptake by DPS and MDPS is shown in Fig. A5. Its removal efficiency increased with the increase of solution temperature for both adsorbents indicating that Cr(VI) sequestration process is endothermic. It is believed that sequestration of Cr(VI) by agrowastes is determined by a reduction step, which is endothermic [23]. Fig. A6 shows that the extent of change in MB removal was positive, proving once more that microemulsion modification enhances the sequestration of MB. However, the extent of that enhancement decreased as the solution temperature increased and became negligible at 60°C. Therefore, it would be recommended that the sequestration of MB by MDPS to be carried on at ambient temperature. The extent of change in Cr(VI) was once more negative due to microemulsion modification, and the increase of solution temperature almost has no effect on such extent.

3.2.3. Isotherm studies

The sequestration of MB onto DPS was modelled using Langmuir isotherm either in its linearised or actual form. The linearised form of Langmuir isotherm (Fig. A7) produced two distinguished straight lines; the first line obtained at the first four initial MB concentrations (50–200 mg L^{-1}), whilst the second line obtained at the last four initial MB concentrations (300–900 mg L^{-1}). The presence of two straight lines indicates the existence of two different types of adsorption sites with a wide spectrum of binding energies on the surface of DPS, where the surface sites with the highest energy to be occupied first [11]. This behaviour could be explained as follows: (i) the Coulombic attraction between DPS surface and MB molecules decreases as the surface charge becomes more positive due to the sequestration of the positively charged MB molecules, (ii) there are unfavourable chemical interactions between adjacent adsorbed MB molecules and (iii) there are variety of site types on the adsorbent surface. Kyzas et al. [31] explained that the deviation from linearity happens when all available monolayer sites are occupied; then some fresh internal surface is created as a result of the pressure of adsorbate molecules forcing into the mesopore and micropore structures. Moreover, MB molecules can be linked to molecular wedges creating access to new surfaces, increasing further the adsorption capacity of DPS. Hence, this process will cause a change in the rate and extent of sequestration and thusly create two linear regions.

Due to the presence of two linear regions, the non-linear regression of MB–DPS isotherm using the actual form of Langmuir isotherm was carried out by dividing the experimental data into two sets. Different error functions were applied, and the function that produced the lowest SNE was selected. The set of isotherm parameters predicted by that function would provide the closest fit to the measured data. A summary of the different sets of isotherm parameters according to different error functions is given in Table A1. The lowest SNE value was obtained when the HYBRID error function was applied. Also, Langmuir isotherm parameters for the whole range of MB concentrations (50–900 mg L^{-1}) are

shown in Table A2. The lowest value of SNE was obtained when MPSD error function was used.

The comparison between the fittings of the two models of Langmuir isotherm is shown in Fig. 6. The one-range model overestimated the values of q_e corresponding to the last two concentrations of the first range. However, it showed good fitting for the second-range data.

The value of b parameter of Langmuir isotherm indicates the affinity of the adsorbent to the adsorbate, and it is related to the free energy of adsorption (i.e. Gibbs free energy). Therefore, if the value of b of an adsorbent is greater than that of another under the same experimental conditions (especially temperature), the adsorbent with the higher value of b will be more favourable. The value of b for the first range of MB initial concentrations was higher than that for the second range of MB initial concentrations. That would confirm that the active sites with higher energy were occupied first, and thusly, new adsorption area would be created but with lower free energy of adsorption and hence lower value of b.

The main adsorption mechanism of MB onto DPS is mainly due to the parallel alignment of MB molecules with the adsorbent surface, and hence, the adsorption of MB can be used to estimate the surface area of an adsorbent. Based on BET surface area of DPS of 80.49 $m^2 g^{-1}$, the molecular area of MB molecule is much less than the cited ranges from 0.69 to 2.10 nm^2. Therefore, other adsorption mechanisms of MB onto DPS are suggested based on hydrophobic interactions, which will create agglomerates of MB molecules on DPS surface [32]. Ferrero [33] suggested that the agglomeration of MB on a charged surface would usually happen at high MB loading, which would be the case in our research. At such high loadings, the MB cations would be tilted nearly perpendicular with respect to the adsorbent surface rather than arranged parallel with the layer plane. Such perpendicular orientation of MB cations would enable a better alignment of adjacent aromatic rings of neighbouring cations via hydrophobic interactions. This would also allow formation of large agglomerates on the adsorbent surface, and simultaneously, each MB cation would be electrostatically bound to negatively charged functional groups. Therefore, it would be expected that at low MB initial concentrations (50–200 mg L^{-1}), the two orientations would be possible leading to a relative high adsorption capacity (q_{max} = 109.9 mg g^{-1}). On the other hand, for the range of high MB initial concentrations (300–900 mg L^{-1}), DPS was still capable to adsorb more dye molecules indicating that the main orientation of MB molecules would be perpendicular to DPS surface and increasing the adsorption capacity to 285.6 mg g^{-1}. Such behaviour would also explain the presence of two distinguished ranges regarding MB adsorption isotherm.

The adsorption isotherm of MB onto MDPS was best fit using one-range Langmuir isotherm model as can be seen in Fig. 7. The best fitting was achieved using HYBRID error function, which resulted in the lowest value of SNE as can be seen in Table A3. It seems that the microemulsion modification of DPS resulted in increasing the homogeneity of the new created surface. It is expected that microemulsion micelles to cover most of DPS surface, and therefore, the main active functional group would be the surfactant, leading to uniform adsorption energy.

The microemulsion modification of DPS enhanced the adsorption of MB, which can be concluded from the significant increase in q_{max} to 555.0 mg g^{-1}. Also, the favourability of MB adsorption by MDPS can be proven since the value of b has increased significantly after the modification. Finally, since the presence of two distinguished regions disappeared after the modification, it is expected that the perpendicular orientation of MB molecules is predominant, and hence, the main adsorption mechanism of MB by MDPS would be hydrophobic attraction.

The adsorption of Cr(VI) onto DPS was modelled by Langmuir isotherm, which demonstrated the presence of two distinguished linear ranges (Fig. A8). The parameters of the two models of Langmuir isotherm with error analysis are presented in Tables A4 and A5. The two-range Langmuir isotherm gave the best fitting of the experimental adsorption data with the lowest values of SNE. The value of Langmuir parameter of b for the second range was lower than that for the first range, confirming that the adsorption sites with highest energy would be utilised firstly. Finally, the fittings of the two models of Langmuir isotherm for the adsorption

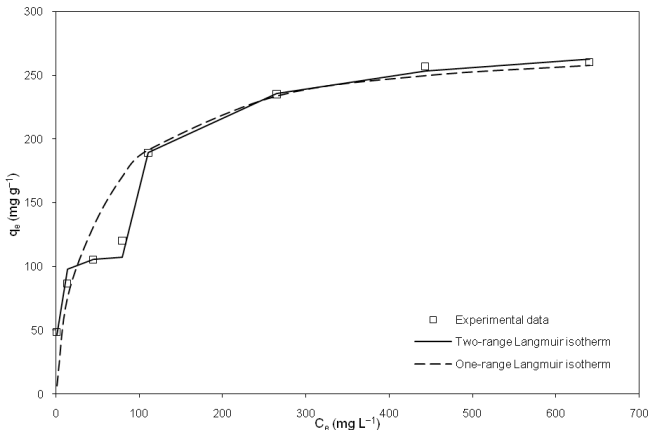

Fig. 6. Comparison of the fittings of the two models of Langmuir isotherm for the adsorption of MB onto DPS (experimental conditions: mass of DPS = 0.05 g, volume of solution = 50 mL, equilibrium time = 72 h, temperature = 20°C, shaking speed = 100 rpm and solution pH = 8.0).

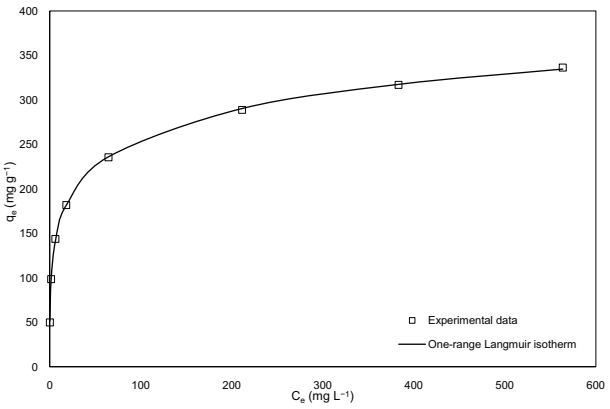

Fig. 7. Fitting of MB adsorption onto MDPS using one-range Langmuir isotherm (experimental conditions: mass of MDPS = 0.05 g, volume of solution = 50 mL, equilibrium time = 72 h, temperature = 20°C, shaking speed = 100 rpm and solution pH = 8.0).

of Cr(VI) onto DPS are presented in Fig. 8. The one-range Langmuir model was not able to predict the experimental data for the last five concentrations, and from Table A5, it can be seen that the one range of the Langmuir isotherm was not capable of providing suitable fitting since some of the estimated parameters were unrealistic even at low values of SNE. Therefore, the most realistic values of the parameters were estimated using the linearised form of the two-range Langmuir isotherm regardless of the value of SNE.

The removal of Cr(VI) by MDPS was studied at solution pH of 2.0 since Cr(VI) adsorption is highly sensitive to solution pH. It was shown that the microemulsion modification caused a shift in the optimal value of solution pH from 3.0 to 2.0, signifying that the solution acidity would be the controlling parameter for Cr(VI) uptake by MDPS. In other words, Cr(VI) adsorption mechanism by DPS might be due to interaction between chromium anionic compounds and

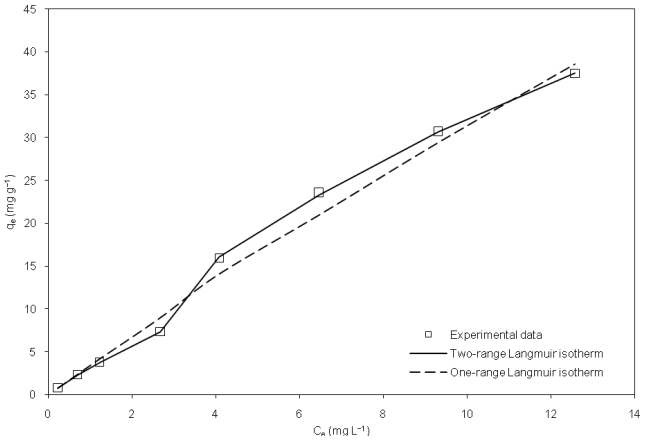

Fig. 8. Comparison of the fittings of the two models of Langmuir isotherm for the adsorption of Cr(VI) onto DPS (experimental conditions: mass of DPS = 0.05 g, volume of solution = 50 mL, equilibrium time = 72 h, temperature = 20°C, shaking speed = 80 rpm and solution pH = 3.0).

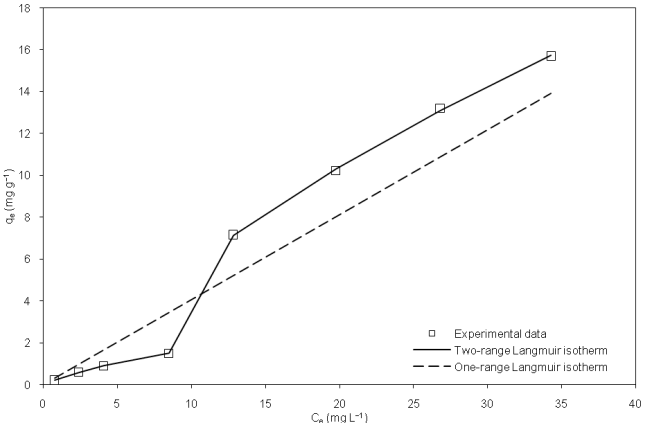

Fig. 9. Comparison of the fittings of the two models of Langmuir isotherm for the adsorption of Cr(VI) onto MDPS (experimental conditions: mass of MDPS = 0.05 g, volume of solution = 50 mL, equilibrium time = 72 h, temperature = 20°C, shaking speed = 80 rpm and solution pH = 2.0).

positively charged parts of surface functional groups with the possibility of reducing those compounds to Cr^{3+} and then adsorbed by negative charged parts of surface functional groups. Whilst for MDPS, adsorbent surface would be mainly covered by surfactant molecules ($RCOO^-Na^+$) indicating that the main removal mechanism of Cr(VI) would be ion exchange. To achieve that, Cr(VI) anionic compounds are reduced by H^+ ions to Cr^{3+} and then ionic exchanged with three cations of Na^+. That would explain the need of lower solution pH to provide higher concentration of H^+ ions. Due to that, the adsorption capacities of Cr(VI) by MDPS were lower than that of DPS as shown in Table A6. Once more, the one-range Langmuir isotherm was not capable to fit the experimental data since the values of q_{max} estimated from non-linear regression were totally unrealistic as can be seen in Table A7.

A comparison between the fittings of the two models of Langmuir isotherm is shown in Fig. 9. It is noticed that values of q_e corresponding to the low range of initial concentrations of Cr(VI) (1–10 mg L^{-1}) were significantly lower than those of Cr(VI) adsorption onto DPS (Fig. 8). That would be due to the high acidity of the solution, which would provide H^+ ions greater than needed to reduce the entire amount of Cr(VI) anionic compounds, and hence, the remained H^+ ions would compete with Cr^{3+} ions to be exchanged with Na^+. The Pauling's electronegativity of H^+ ions is 2.20 and higher than that of Cr^{3+}, which is 1.66. Due to that, the ion exchange rate between H^+ and Na^+ ions would be higher and thusly reducing the total chromium adsorption capacity. The value of adsorption capacity, q_{max}, for the first range was considerably low (3.843 mg g^{-1}), almost 7% of q_{max} for the second range (56.25 mg g^{-1}).

The two-range Langmuir isotherm gave the best fitting of Cr(VI) adsorption onto MDPS. The microemulsion modification of DPS would reduce its surface heterogeneity. But due to the different chemical bonding between the microemulsion molecules and surface functional groups, the adsorption energy would be uneven and might be divided into two sets and, hence, the two values of Langmuir isotherm energy-related parameter (b).

Langmuir isotherm is usually used to predict the monolayer maximum adsorption capacity, q_{max}, for different adsorbents. However, these predictions are intensively depending firstly on the fitting accuracy and secondly on the experimental conditions. Generally, the fitting criteria is the correlation factor, R^2, which is easily abused since it is sensitive to extreme data points that are further complicated with Langmuir linearisation [34]. Also, the values of q_{max} depend on the experimental conditions, such as solution pH and temperature, adsorbent particle size, adsorbent surface modification, presence of different ions in solutions, etc. For example, Cr(VI) adsorption would be highly deteriorated by slight change in solution pH, and if the adsorption mechanism involved reduction of chromium anionic compounds, the increase of the solution temperature would increase the adsorption capacity. Therefore, if the values of q_{max} of different adsorbents to be compared, this comparison should be treated with caution. Even though, such comparison can be used as a loose guide to determine the advantages of using low-cost adsorbents over CACs. Therefore, values of q_{max} of CACs and agrowastes are compared with those predicted in this

Table 4
The monolayer maximum adsorption capacity, q_{max}, of MB onto different adsorbents

Adsorbents	q_{max} (mg g^{-1})	Comments
Commercial activated carbon (AC)	980.3	Solution pH = 7.4, dose = 2 g L^{-1}, speed = 200 rpm, contact time = 35 min, particle size = 90 μm, concentration = 600–900 mg L^{-1}
MDPS	555.0	Present study
Filtrasorb 400 AC	476	Solution pH = 9, dose = 1 g L^{-1}, concentration = 100–800 mg L^{-1}, particle size < 106 μm, temperature = 20°C
Rice husk	312.26	Contact time = 6 h, concentration = 10–1,000 mg L^{-1}, temperature = 20°C, particle size = 242.2 μm
Filtrasorb 400 AC	295	Dose = 1 g L^{-1}, contact time = 30 min, concentration = 200–500 mg L^{-1}, temperature = 25°C, particle size < 66 μm, Solution pH uncontrolled
Cotton waste	277.77	Contact time = 6 h, concentration = 10–1,000 mg L^{-1}, temperature = 20°C, particle size = 5–10 mm
DPS	277.6	Present study
Norit AC	276	Dose = 1 g L^{-1}, contact time = 30 min, concentration = 200–500 mg L^{-1}, temperature = 25°C, particle size < 66 μm, Solution pH uncontrolled
Banana stalk waste	243.90	Solution pH = 7, dose = 1 g L^{-1}, contact time = 330 min, concentration = 50–500 mg L^{-1}, temperature = 30°C, particle size = 0.5–1 mm, shaking speed = 100 rpm
Palm kernel fibre	217.95	Solution pH = 7.1, dose = 0.67 g L^{-1}, contact time = 360 min, concentration = 10–550 mg L^{-1}, temperature = 26°C, particle size = 50–60 μm, shaking speed = 80 rpm
H_3PO_4-modified rice straw	208.33	Natural solution pH, dose = 2 g L^{-1}, contact time = 6 h, concentration = 50–350 mg L^{-1}, temperature = 20°C ± 2°C, shaking speed = 150 rpm
Commercial AC	200	Solution pH = 6.94, dose = 4 g L^{-1}, contact time = 30 min, concentration = 100–1,000 mg L^{-1}, temperature = 24°C
Cedar sawdust	142.36	Solution pH = 7.1, adsorbent mass = 0.001–0.015 g, solution volume = 10 mL, contact time = 5 h, concentration = 40 mg L^{-1}, temperature = 20°C, particle size = 80–315 μm, shaking speed = 400 rpm
Meranti sawdust	120.48	Solution pH = 9, dose = 5 g L^{-1}, a contact time = 3 h, concentration = 50–200 mg L^{-1}, temperature = 30°C, particle size = 100–150 μm, shaking speed = 150 rpm
Coffee husks	90.1	Solution pH = 8, dose = 10 g L^{-1}, concentration = 50–500 mg L^{-1}, temperature = 30°C, shaking speed = 100 rpm
RDP	80.29	Dose = 5 g L^{-1}, concentration = 20–400 mg L^{-1}, particle size 125–212 μm, temperature = 25°C, contact time = 24 h
Ground hazelnut shells	76.9	Solution pH = 8, dose = 1 g L^{-1}, concentration = 250–1,000 mg L^{-1}, temperature = 20°C, particle size = 125 μm, shaking speed = 60 rpm
Walnut sawdust	59.17	
Cherry sawdust	39.84	
Oak sawdust	29.94	
Pitch-pine sawdust	27.78	
Banana peel	20.8	Solution pH = 7.2, dose = 1 g L^{-1}, contact time = 24 h, concentration = 10–120 mg L^{-1}, temperature = 30°C, shaking speed = 180 rpm
Orange peel	20.3	
Activated date pits (900°C)	17.27	Dose = 5 g L^{-1}, concentration = 20–400 mg L^{-1}, particle size = 125–212 μm, temperature = 25°C, contact time = 24 h
Activated date pits (500°C)	12.94	

research. The values of q_{max} for MB adsorption onto different adsorbents are compared in Table 4 where all the reported values for other adsorbents were taken from Rafatullah et al. [35]. For Cr(VI), the comparison is given in Table 5 where all the reported values for other adsorbents were taken from Hubbe et al. [36]. Also, some comments were given regarding experimental conditions when available.

The tabulated q_{max} values of MB showed that the q_{max} of MDPS was the second best value and it was higher than some CACs. Also, the q_{max} of RDP was in the top ten values, and the only two better agrowastes were rice husk and cotton waste. Therefore, it could be concluded that use of MDP and DPS to remove MB from aqueous solutions had a great potential over other agrowastes.

Table 5
The monolayer maximum adsorption capacity, q_{max}, of Cr(VI) onto different adsorbents

Adsorbents	q_{max} (mg g^{-1})	Comments
DPS	85.95	Present study
Cocoa shells	53	Solution pH = 2, particle size = 1–30 mm, solution volume = 200 mL, dose = 5–40 g L^{-1}, contact time = 24 h, temperature = 22°C–24°C, shaking speed = 150 rpm
Commercial AC	44.44	Solution pH = 2, particle size = 0.65 mm, dose = 0.8 g L^{-1}, concentration = 100–1,000 mg L^{-1}, contact time = 48 h, temperature = 22°C, shaking speed = 150 rpm
MDPS	42.54	Present study
Wool	41.15	Wool particle size = 1 cm, other adsorbents' particle size = 200 μm, solution pH = 2, dose = 8 g L^{-1}, contact time = 2 h, concentration = 20–1,000 mg L^{-1}, temperature = 30°C
Olive cake	33.44	
Sawdust	15.28	
Pine needles	21.50	
Almond	10.62	
Coal	6.78	
Dyestuff-treated rice hulls	39.7	Particle size < 2 mm, solution volume = 50 mL, adsorbent mass = 0.5 g, contact time = 2 h
(red and yellow)	39.1	
Acorn	31.5	Solution pH = 2
Pine bark, cones and needles	22	Smaller particles higher uptake. Solution pH = 2
CH_2O-modified rosewood	23	Solution pH = 3
Hazelnut shells	18	Solution pH = 2.5–3.5
Olive stone	15	Higher temperature favoured. Solution pH = 2–3
Maple sawdust	5	Solution pH = 6
Conifer needles	6.3	Solution pH = 3
Rice husk	6–10	Solution pH = 2

Table 6
Percentages of MB, Cd(II), Cu(II) and Cr(VI) desorption from DPS and MDPS

DPS		
Desorption (%)		
Eluent	MB	Cr(VI)
H_2O	0.619	0.411
NaOH (1 M)	0.789	31.78
HCl (1 M)	4.041	2.007
MDPS		
Desorption (%)		
	MB	Cr(VI)
H_2O	0.665	0.443
NaOH (1 M)	0.521	22.94
HCl (1 M)	3.161	1.870
Extent of change (%) due to microemulsion modification		
	MB	Cr(VI)
H_2O	+7.431	+7.786
NaOH (1 M)	–33.97	–27.82
HCl (1 M)	–21.78	–6.826

Regarding the adsorption capacities of Cr(VI), the revised values in Table 5 showed that the q_{max} of DPS was the highest, whilst the q_{max} of MDPS was higher than most of the reported agrowastes. Finally, the experimental conditions reported in Table 5 show that the optimal solution pH for Cr(VI) adsorption would be between 2 and 3, similar to those used in this research.

When a process of adsorption is studied, it is very important to ascertain if it is a reversible process or not. Investigating the extent of desorption is essential to examine the potential to recover adsorbed compounds and the adsorbent regeneration for successive reuse [23]. The desorption percentages of MB and Cr(VI) by each eluent are listed in Table 6. For MB, the acidic solution of HCl showed higher desorption percentage than neutral and basic solutions. However, none of the eluents gave substantial desorption percentages, indicating that the bonding of MB molecules to the surface of DPS or MDPS was strong. Sites with high bonding energy create stable bonds leading to an irreversible adsorption process, and hence, chemisorption might here be the major adsorption mechanism [37,38]. The neutral and acidic eluents gave very low desorption percentages of Cr(VI), whilst the basic solution (1 M NaOH) generated the largest desorption percentages, confirming that adsorption mechanism of Cr(VI) by DPS or MDPS was totally different than that of MB. Finally, desorption from MDPS was lower, proposing that the interactions between these pollutants and MDPS surface are stronger than those with DPS surface.

Desorption studies can elucidate the adsorption mechanism of pollutants by assessing their extraction using different eluents. For Cr(VI), alkaline solutions gave the lowest removal efficiencies. Therefore, using alkaline solutions will weaken the adsorption forces and consequently facilitate the elution and the release of adsorbed chromium ions into the aqueous solution. The adsorption of chromium involves several mechanisms including chemisorption, which is an irreversible process. Since the desorption of Cr(VI) from

MDPS or DPS by 1 M NaOH ranged from 23% to 31%, the chemisorption mechanism might still be significant. On the other hand, the highest desorption of MB was achieved by HCl, indicating the involvement of ion-exchange process in its adsorption. Even though, MB desorption percentages were very low because its main adsorption mechanism was chemisorption.

4. Conclusions

In this investigation, DPS showed higher negative surface charges and lower pH_{ZPC} value compared with microemulsion-MDPS, concluding that the surface of MDPS was more basic than DPS. Moreover, the attachment mechanism of microemulsion molecules to the DPS surface would be either by the hydrophilic part or by the hydrophobic part of the surfactant molecule, and therefore, the nature of MDPS surface cannot be simply described either as hydrophilic or hydrophobic. The microemulsion modification considerably reduced the surface area and total pore volume of the unmodified stones, where the large size of the microemulsion molecules would block DPS micropores. That was confirmed since the fraction of the micropore volume to the total pore volume of DPS of 63% drastically decreased to <1% after microemulsion modification.

The effect of microemulsion modification on the sequestration of MB and Cr(VI) from aqueous solution was investigated under different operating conditions. The sequestration of Cr(VI) was highly dependent on the solution pH, and its effect was more noticed after the microemulsion modification, where the optimal solution pH shifted to further acidic conditions. The microemulsion modification changed the thermodynamic nature of MB sequestration process from endothermic by DPS to exothermic by MDPS. Even though, the removal efficiency of MB by MDPS at different solution temperatures was still higher. However, the thermodynamic nature of Cr(VI) sequestration process has not changed after the microemulsion modification. The microemulsion-MDPS showed higher adsorption capacity of MB but showed lower capacity of Cr(VI).

Acknowledgement

The authors would like to acknowledge QUESTOR centre and the School of Chemistry and Chemical Engineering at Queen's University of Belfast for their technical support, especially providing an access to their own analytical equipment.

References

[1] A. Hans, A. Bharat, Water as a resource: different perspectives in literature, Int. J. Eng. Res. Technol., 3 (2014) 27–34.
[2] S.H. Abbas, I.M. Ismail, T.M. Mostafa, A.H. Sulaymon, Biosorption of heavy metals: a review, J. Chem. Sci. Technol., 3 (2014) 74–102.
[3] A. Jaafar, A. Boussaoud, Disappearance of Basic yellow 28 from aqueous solution by Fenton's reagent, J. Mater. Environ. Sci., 5 (2014) 2426–2431.
[4] H.D. Beyene, The potential of dyes removal from textile wastewater by using different treatment technology, a review, Int. J. Environ. Monit. Anal., 2 (2014) 347–353.
[5] G.Z. Kyzas, M. Kostoglou, Green adsorbents for wastewater: a critical review, Materials, 7 (2014) 333–364.
[6] M.Z. Hossain, M.I. Waly, V. Singh, V. Sequeira, M.S. Rahman, Chemical composition of date-pits and its potential for developing value-added product – a review, Pol. J. Food Nutr. Sci., 64 (2014) 215–226.
[7] T. Ahmad, M. Danish, M. Rafatullah, A. Ghazali, O. Sulaiman, R. Hashim, M.N.M. Ibrahim, The use of date palm as a potential adsorbent for wastewater treatment: a review, Environ. Sci. Pollut. Res., 19 (2012) 1464–1484.
[8] M.A. Al-Ghouti, A. Hawari, M. Khraisheh, A solid-phase extractant based on microemulsion modified date pits for toxic pollutants, J. Environ. Manage., 130 (2013) 80–89.
[9] P. Malakul, K.R. Srinivasan, H.Y. Wang, Metal adsorption and desorption characteristics of surfactant modified clay complexes, Ind. Eng. Chem. Res., 37 (1998) 4296–4301.
[10] T.N. Dantas, A.A. Dantas Neto, M.C. Moura, Removal of chromium from aqueous solutions by diatomite with microemulsion, Water Res., 35 (2001) 2219–2224.
[11] M.A.M. Khraisheh, M.S. Al-Ghouti, Enhanced dye adsorption by microemulsion-modified calcined diatomite (mμ-CD), Adsorption, 11 (2005) 547–559.
[12] Y.S. Al-Degs, A.H. El-Sheikh, M.A. Al-Ghouti, B. Hemmateenejad, G.M. Walker, Solid-phase extraction and simultaneous determination of trace amounts of sulphonated and azo sulphonated dyes using microemulsion-modified-zeolite and multivariate calibration, Talanta, 75 (2008) 904–915.
[13] X. Xin, J. Wang, H. Yu, B. Du, Q. Wei, L. Yan, Removal of o-nitrobenzoic acid by adsorption on to a new organoclay: montmorillonite modified with HDTMA microemulsion, Environ. Technol., 32 (2011) 447–454.
[14] D. Dollimore, G.R. Heal, An improved method for the calculation of pore size distribution from adsorption data, J. Appl. Chem., 14 (1964) 109–114.
[15] O.D. Narety, B. Zhao, Biochar preparation, characterization, and adsorptive capacity and its effect on bioavailability of contaminants: an overview, Adv. Mater. Sci. Eng., 2014 (2014) 12.
[16] S. Rajkumar, S. Murugesh, V. Sivasankar, A. Darchen, T.A.M. Msagati, T. Chaabane, Low-cost fluoride adsorbents prepared from a renewable biowaste: synthesis, characterisation and modeling studies, Arabian J. Chem. (2015), http://dx.doi.org/10.1016/j.arabjc.2015.06.028 (in press)
[17] F. Raji, A. Saraeian, M. Pakizeh, F. Attarzadeh, Removal of Pb(II) from aqueous solution by mesoporous silica MCM-41 modified by $ZnCl_2$: kinetics, thermodynamics, and isotherms, RSC Adv., 5 (2015) 37066–37077. doi: 10.1039/C5RA01192B.
[18] I.E. Grossman, J. Viswanathan, A. Vecchietti, R. Raman, E. Kalvelagen, GAMS – The Solver Mauals, GAMS Development Corporation, Washington, D.C., USA, 2008.
[19] H.H. Sait, A. Hussain, A.A. Salema, F.N. Ani, Pyrolysis and combustion kinetics of date palm biomass thermogravimetric analysis, Bioresour. Technol., 118 (2012) 382–389.
[20] M. Gorgievski, D. Božić, V. Stanković, N. Štrbac, S. Šerbula, Kinetics, equilibrium and mechanism of Cu^{2+}, Ni^{2+} and Zn^{2+} ions biosorption using wheat straw, Ecol. Eng., 58 (2013) 113–122.
[21] A. Cid, O.A. Moldes, J. Morales, J.C. Mejuto, Effects of additives upon percolation temperature in AOT-based microemulsions, J. Appl. Sol. Chem. Model., 3 (2014) 106–129.
[22] A. Abdolali, W.S. Guo, H.H. Ngo, S.S. Chen, N.C. Nguyen, K.L. Tung, Typical lignocellulosic wastes and by-products for biosorption process in water and wastewater treatment: a critical review, Bioresour. Technol., 160 (2014) 57–66.
[23] A.B. Albadarin, A.H. Al-Muhtaseb, N.M.A. Al-laqtah, G.M. Walker, S.J. Allen, M.N.M. Ahmad, Biosorption of toxic chromium from aqueous phase by lignin: mechanism, effect of other metal ions and salts, Chem. Eng. J., 169 (2011) 20–30.
[23] Y. Zhang, S. Yang, J.Q. Wu, T.Q. Yuan, R.C. Sun, Preparation and characterization of lignocellulosic oil sorbent by hydrothermal treatment of *Populus* fiber, Materials, 7 (2014) 6733–6747. doi: 10.3390/ma7096733.
[24] A. Zhang, C. Liu, J. Xie, R. Sun, Homogeneous derivatization of sugarcane bagasse with Myristyl Chloride at room temperature to prepare bio-based oil adsorbents, BioResources, 10 (2015) 887–897.

[25] M. Soleymanzadeh, M. Arshadi, J.W.L. Salvacion, F. SalimiVahid, A new effective nanobiocomposite for sequestration of Cd(II) ions: nanoscale zerovalent iron supported on sineguelas seed waste, Chem. Eng. Res. Des., 93 (2015) 696–709.
[26] L.A. Sepúlveda, F.A. Cuevas, E.G. Contreras, Valorization of agricultural wastes as dye adsorbents: characterization and adsorption isotherms, Environ. Technol., 36 (2015) 1913–1923. doi: 10.1080/09593330.2015.1016119.
[27] N. Stevulova, J. Cigasova, A. Estokova, E. Terpakova, A. Geffert, F. Kacik, E. Singovszka, M. Holub, Properties characterization of chemically modified hemp hurds, Materials, 7 (2014) 8131–8150. doi: 10.3390/ma7128131.
[28] O. Gordobil, I. Egüés, I. Urruzola, J. Labidi, Xylan-cellulose films: improvement of hydrophobicity, thermal and mechanical properties, Carbohydr. Polym., 112 (2014) 56–62.
[29] J. Nilsen-Nygaard, S.P. Strand, K.M. Vårum, K.I. Draget, C.T. Nordgård, Chitosan: gels and interfacial properties, Polymers, 7 (2015) 552–279. doi: 10.3390/polym7030552.
[30] B. Acevedo, C. Barriocanal, I. Lupul, G. Gryglewicz, Properties and performance of mesoporous activated carbons from scrap tyres, bituminous wastes and coal, Fuel, 151 (2015) 83–90.
[31] G.Z. Kyzas, P.I. Siafaka, E.G. Pavlidou, K.J. Chrissafis, D.N. Bikiaris, Synthesis and adsorption application of succinyl-grafted chitosan for the simultaneous removal of zinc and cationic dye from binary hazardous mixtures, Chem. Eng. J., 259 (2015) 438–448.
[32] Y. Qi, A.F.A. Hoadley, A.L. Chaffee, G. Garnier, Characterisation of lignite as an industrial adsorbent, Fuel, 90 (2011) 1567–1574.
[33] F. Ferrero, Adsorption of methylene blue on magnesium silicate: kinetics, equilibria and comparison with other adsorbents, J. Environ. Sci., 22 (2010) 467–473.
[34] M.I. El-Khaiary, G.F. Malash, Common data analysis errors in batch adsorption studies, Hydrometallurgy, 105 (2011) 314–320.
[35] M. Rafatullah, O. Sulaiman, R. Hashim, A. Ahmad, Adsorption of methylene blue on low-cost adsorbents: a review, J Hazard. Mater., 177 (2010) 70–80.
[36] M.A. Hubbe, S.H. Hasan, J.J. Ducoste, Cellulosic substrates for removal of pollutants from aqueous systems: a review. 1. Metals, BioResources, 6 (2011) 2161–2287.
[37] D. Kavitha, C. Namasivayam, Experimental and kinetic studies on methylene blue adsorption by coir pith carbon, Bioresour. Technol., 98 (2007) 14–21.
[38] A.B. Albadarin, C. Mangwandi, G.M. Walker, S.J. Allen, M.N. Ahmad, Biosorption characteristics of sawdust for the removal of Cd(II) ions: mechanism and thermodynamic studies, Chem. Eng. Trans., 5 (2011) 1297–1302.

Appendix A

Supplementary figures and tables

A.1. Effect of solution pH

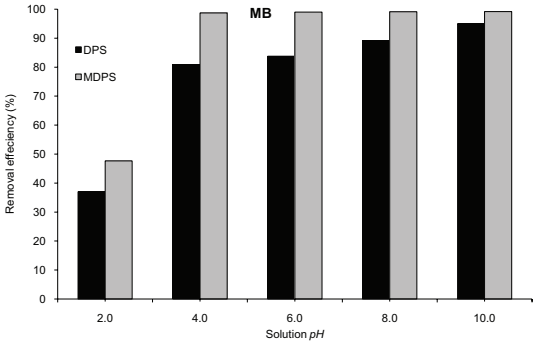

Fig. A1. Solution pH dependency of MB removal by DPS and MDPS (experimental conditions: mass of adsorbent = 0.05 g, volume of solute solution = 50 mL, equilibrium time = 96 h, shaking speed = 150 rpm, temperature = 20°C, initial concentration = 100 mg L^{-1}).

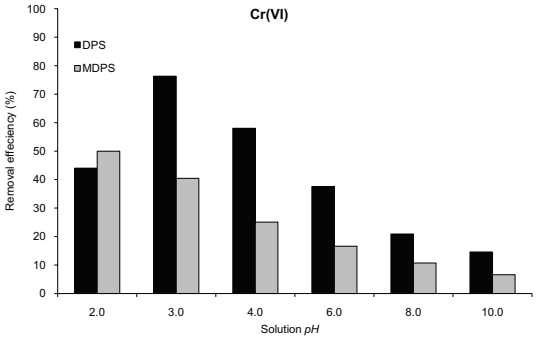

Fig. A2. Solution pH dependency Cr(VI) removal by DPS and MDPS (experimental conditions: mass of adsorbent = 0.05 g, volume of solute solution = 50 mL, equilibrium time = 96 h, shaking speed = 150 rpm, temperature = 20°C, initial concentration = 50 mg L^{-1}).

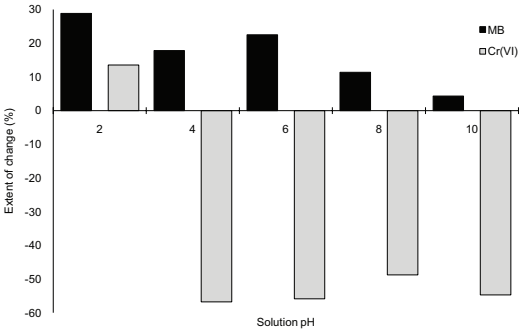

Fig. A3. Extent of change in the removal efficiency of MB and Cr(VI) at different solution pH due to microemulsion modification of DPS.

A.2. Effect of solution temperature

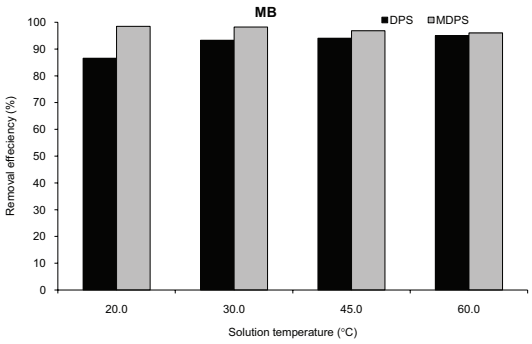

Fig. A4. Effect of solution temperature on the removal efficiencies of MB by DPS and MDPS (experimental conditions: mass of adsorbent = 0.05 g, volume of solution = 50 mL, equilibrium time = 96 h, shaking speed = 150 rpm, solution pH = 8.0, initial concentration = 100 mg L^{-1}).

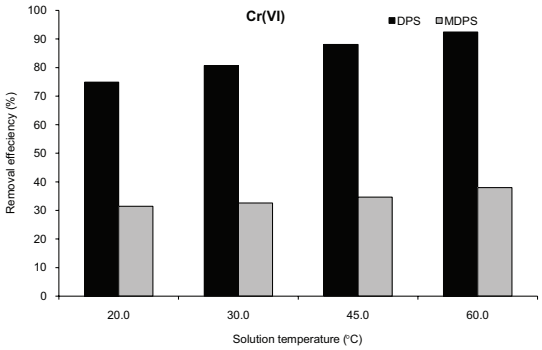

Fig. A5. Effect of solution temperature on the removal efficiencies of Cr(VI) by DPS and MDPS (experimental conditions: mass of adsorbent = 0.05 g, volume of solution = 50 mL, equilibrium time = 96 h, shaking speed = 150 rpm, solution pH = 3.0 for DPS and 2.0 for MDPS, initial concentration = 50 mg L^{-1}).

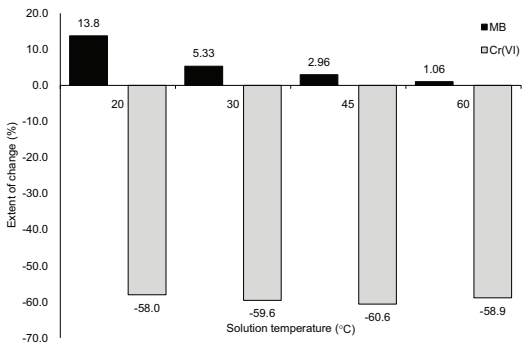

Fig. A6. Extent of change in removal efficiency of MB and Cr(VI) at different solution temperatures due to microemulsion modification of DPS.

A.3. Adsorption equilibrium isotherms

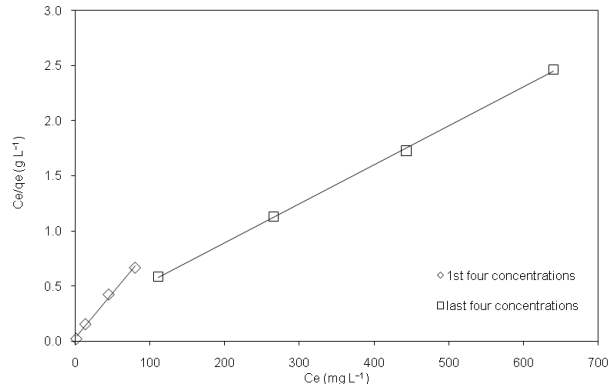

Fig. A7. Adsorption isotherm of MB onto DPS after linearizing Langmuir isotherm model (experimental conditions: mass of DPS = 0.05 g, volume of solution = 50 mL, equilibrium time = 72 h, temperature = 20°C, shaking speed = 100 rpm and solution pH = 8.0).

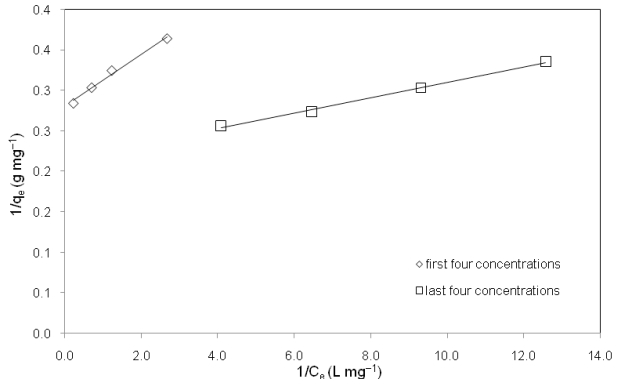

Fig. A8. Adsorption isotherm of Cr(VI) onto DPS after linearizing Langmuir isotherm model (experimental conditions: mass of RDP = 0.05 g, volume of solution = 50 mL, equilibrium time = 72 h, temperature = 20°C, shaking speed = 80 rpm and solution pH = 3.0).

Table A1
Two-range Langmuir isotherm parameters for MB adsorption onto DPS

First range of MB initial concentrations (50–200 mg L^{-1})					
	Linearised form	SSE	HYBRID	MPSD	RMSE
b (L mg^{-1})	0.633	0.560	0.633	0.680	0.560
q_{max} (mg g^{-1})	109.6	111.7	109.9	107.7	111.7
SNE	3.832	3.618	3.525	3.622	3.618
Second range of MB initial concentrations (300–900 mg L^{-1})					
	Linearised form	SSE	HYBRID	MPSD	RMSE
b (L mg^{-1})	0.018	0.018	0.018	0.018	0.018
q_{max} (mg g^{-1})	285.6	285.6	285.6	290.7	285.6
SNE	1.286	1.287	1.286	4.000	1.287

Table A2
One-range Langmuir isotherm parameters for MB adsorption onto DPS

Whole range of MB initial concentrations (50–900 mg L^{-1})					
	Linearised form	SSE	HYBRID	MPSD	RMSE
b (L mg^{-1})	0.017	0.020	0.038	0.020	0.014
q_{max} (mg g^{-1})	280.8	277.6	241.1	277.6	291.7
SNE	3.062	3.222	3.993	2.984	3.038

Table A3
One-range Langmuir isotherm parameters for MB adsorption onto MDPS

Whole range of MB initial concentrations (50–900 mg L^{-1})					
	Linearised form	SSE	HYBRID	MPSD	RMSE
b (L mg^{-1})	0.181	0.186	0.186	0.179	0.186
q_{max} (mg g^{-1})	564.2	556.1	555.0	566.5	556.1
SNE	3.626	3.362	3.407	3.884	3.362

Table A4
Two-range Langmuir isotherm parameters for Cr(VI) adsorption onto DPS

First range of Cr(VI) initial concentrations (1–10 mg L^{-1})					
	Linearised form	SSE	HYBRID	MPSD	RMSE
b (L mg^{-1})	0.115	0.102	0.039	0.117	0.102
q_{max} (mg g^{-1})	31.02	34.09	80.00	30.55	34.09
SNE	0.493	0.482	4.000	2.208	0.472
Second range of MB initial concentrations (20–50 mg L^{-1})					
	Linearised form	SSE	HYBRID	MPSD	RMSE
b (L mg^{-1})	0.044	0.045	0.044	0.043	0.045
q_{max} (mg g^{-1})	105.5	103.5	104.9	106.4	103.5
SNE	1.883	2.131	2.926	4.000	2.131

Table A5
One-range Langmuir isotherm parameters for Cr(VI) adsorption onto DPS

Whole range of MB initial concentrations (1–50 mg L^{-1})					
	Linearised form	SSE	HYBRID	MPSD	RMSE
b (L mg^{-1})	0.041	0.004	0.010	0.002	0.026
q_{max} (mg g^{-1})	85.95	791.0	345.5	1,420	156.7
SNE	3.885	1.785	1.141	1.294	1.654

Table A6
Two-range Langmuir isotherm parameters for Cr(VI) adsorption onto MDPS

First range of Cr(VI) initial concentrations (1–10 mg L^{-1})					
	Linearised form	SSE	HYBRID	MPSD	RMSE
b (L mg^{-1})	0.075	0.070	0.020	0.054	0.075
q_{max} (mg g^{-1})	3.843	4.021	11.052	4.868	3.843
SNE	0.140	0.284	4.000	0.746	0.117
Second range of MB initial concentrations (20–50 mg L^{-1})					
	Linearised form	SSE	HYBRID	MPSD	RMSE
b (L mg^{-1})	0.011	0.013	0.013	0.011	0.011
q_{max} (mg g^{-1})	56.07	49.30	51.59	56.25	56.07
SNE	1.436	4.000	2.560	1.435	1.436

Table A7
One-range Langmuir isotherm parameters for Cr(VI) adsorption onto MDPS

Whole range of MB initial concentrations (1–50 mg L^{-1})					
	Linearised form	SSE	HYBRID	MPSD	RMSE
b (L mg^{-1})	6.37E-03	8.90E-06	1.34E-06	1.74E-06	1.11E-05
q_{max} (mg g^{-1})	42.54	53,157	302,058	151,177	42,530
SNE	3.501	1.788	1.647	2.899	1.792